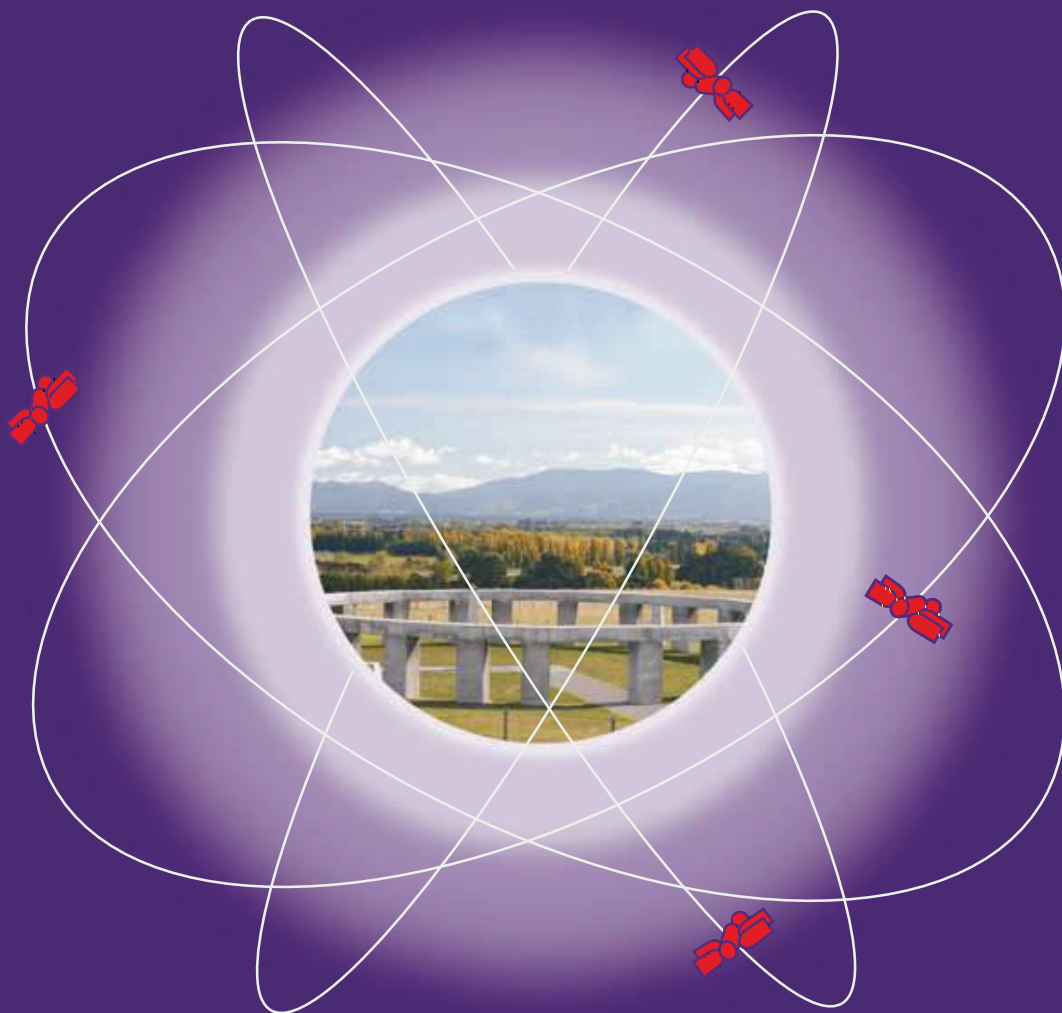


NEW ZEALAND SURVEYOR

Journal of the New Zealand Institute of Surveyors No. 299 2009



- Climate change, local government and the survey profession
- Intensity calibration method for 3D laser scanners
- Lines on the land
- Water level measurement and tidal datum transfer using high rate GPS buoys
- Access to landlocked Maori land

DANIEL WUJANZ

Department of Spatial Sciences, Curtin
University of Technology, GPO Box
U1987, Perth, WA 6845, Australia
D.Wujan@curtin.edu.au

Intensity calibration method for 3D laser scanners

ABSTRACT

A calibration method for intensity values from a 3D laser scanner (Leica HDS 3000) is presented in this paper. Different influences on the returning laser beam by objects were inspected by using different measurement setups whereby subsequent established variances were compensated. In order to assess the quality of the determined design models for the return laser beam of a laser scanner, a practical dataset was corrected by using a developed programme. In addition, a comparison has been made by segmenting an uncorrected and a corrected dataset.

KEYWORDS

3D-Laserscanning, calibration, segmentation, intensity

INTRODUCTION

Terrestrial 3D laser scanning (TLS) has been utilised in various applications where geometric information needs to be captured with high spatial density such as built structures, archaeology, cultural heritage, mining and reverse engineering (Boehler et al 2004, Bae et al 2007, Gordon 2005). 3D laser scanners are capable of capturing geometric and colour information (RGB) for objects, and also the strength of the returned laser beam. Among the information captured from TLS, the usefulness of the intensity value is mainly for target detection as well as for visualising a measured point cloud (Lichti 2002). However, the raw intensity return of laser scanners needs to be calibrated (Pfeifer et al 2007)

The scientific focus in TLS has been mainly directed at the determination and investigation of the accuracy as well as the extraction of geometric features from point clouds (Belton, 2008). Few research projects

have investigated the intensity values of laser scanners. For example, Hoeffle and Pfeifer (2007) utilised a model-driven approach to correct the influences of topographic and atmospheric effects on the intensity value of airborne laser scanners (ALS). In addition, Kaasalainen et al (2007) developed a rigorous approach to classify the surface of glaciers by using the point cloud information including calibrated ALS intensity values. Lichti (2002) analysed the effects of reflecting surface material and investigated the relationship between intensity and distance in order to classify 3D point clouds with the correctly calibrated intensity. Hancock et al (1998) used terrestrial laser scanners' intensity for the detection of obstacles for highway environments to control mobile robots. Lichti (2005) used near infrared intensity in combination with colour information to filter and classify terrestrial laser scanner point clouds. Wang et al (2009) described the potential of intensity data for planar surface segmentation.

This paper presents a calibration method for the intensity values from 3D laser scanners. First, four experiments with a laser scanner (Leica HDS 3000), a camera (Nikon D2Xs), and a monochromator (LOT Oriel Lambda 500), were conducted in order to investigate the relationships between the returned laser beam and the incidence angle of the laser, the distance between a laser scanner and objects, and the radiometric properties of the objects. Using these instruments, a calibration model for the laser scanner is presented. Second, in order to demonstrate the effectiveness of this approach, a segmentation method is used to compare an uncorrected and a corrected point cloud.

EXPERIMENTS

Basically, laser scanners can be conceived as a fast total station (Gordon 2005), which can measure millions of points within minutes. Two major reasons for the incorrect intensity values from a laser scanner can be summarised as:

- Distance and Incidence angles of the laser beam to objects
- Radiometric properties of objects.

In order to investigate the mathematical relationship between the above factors and the returning laser scanner intensity, the following experiments were conducted and a final correction model for the laser intensity values was developed.

PRELIMINARY EXPERIMENT WITH A LEICA HDS 3000 AND A PHOTOGRAMMETRIC CAMERA

To find the relationship between laser spot size and the distance between the scanner and objects where the focus of a photogrammetric camera is fixed, the following experiment was conducted. The experimental setup consisted of a 100 m long test track with marked positions 10 m apart. A white sheet of paper attached to the bottom of a plastic box was used as a projection screen. A scale (a simple ruler) was mounted on the bottom of the box. (Note that the scale should be attached at right angles to the projection direction of the scanner). At each position, the scanner was used to capture the bottom

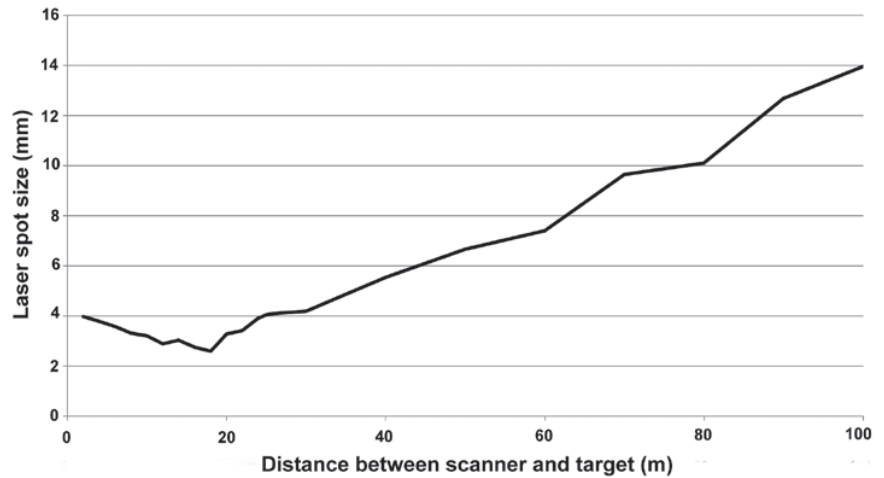


Figure 1: Variation of laser spot size with increasing distance between scanner and target.

Table 1: Statistical comparison between measured and estimated values.

	Standard deviation [%]	Maximum difference [%]
Measured values	2.6	7.8
Modelled values	0.5	1.4

of the box. While the scanning was in progress, 2D images were taken of the scale and the projected laser beam. Because of the high speed the laser spot moved across the object’s surface, the laser spot is difficult to capture. The highest picture rate on the Photogrammetric camera (Nikon D2Xs), eight frames a second, was therefore used. Once all positions and images were captured, the diameter of the laser spot was found by comparing the length of the scale with the laser spot. Although this experiment isn’t accurate enough to determine the exact spot size, it is good enough to show how spot size changes with increasing distance between scanner and target (Figure 1). This does not influence the measured intensity value within the accuracy of the spot size provided by the manufacturer.

Experiment I (Distance vs Intensity)

The purpose of this experiment was to model how a changing distance affects measured laser intensity values. Using a 200m long test track with 10m increments, a planar test object was vertically set on every position. The intensity value at 10m distance is taken as the reference ($= I_{reference}$), and is assumed to be without error. From the measured

intensity at the other points ($= I_{measured}$), an intensity correction for distance is given as:

$$CORRECTION_{distance} = I_{reference} - I_{measured} \quad (1)$$

Least-squares method with a polynomial function (Jaeger et al 2005) shows that:

$$CORRECTION_{distance} \sim 5.7426 \times 10^{-9} \times d^3 - 3.5915 \times 10^{-6} \times d^2 + 9.5578 \times 10^{-4} \times d - 1.4424 \times 10^{-2} \quad (2)$$

where d is the distance between the scanner and the test target in metres. Table 1 shows the results of the approximated as well as the measured values.

Experiment II (Incidence angle vs Intensity)

To investigate the relationship between the incidence angle and the returned intensity from an object, a flat object was irradiated and the incidence angle of the laser beam varied from zero (vertical setup) to approximately 76°. The distance between the flat object and the scanner, and their horizontal orientation, were kept constant. Individual scan lines were extracted out of the 3D point cloud in order to evaluate the difference to the surface normal direction for each point, which resulted in values between

Figure 2: Measured intensity vs modelled intensity.

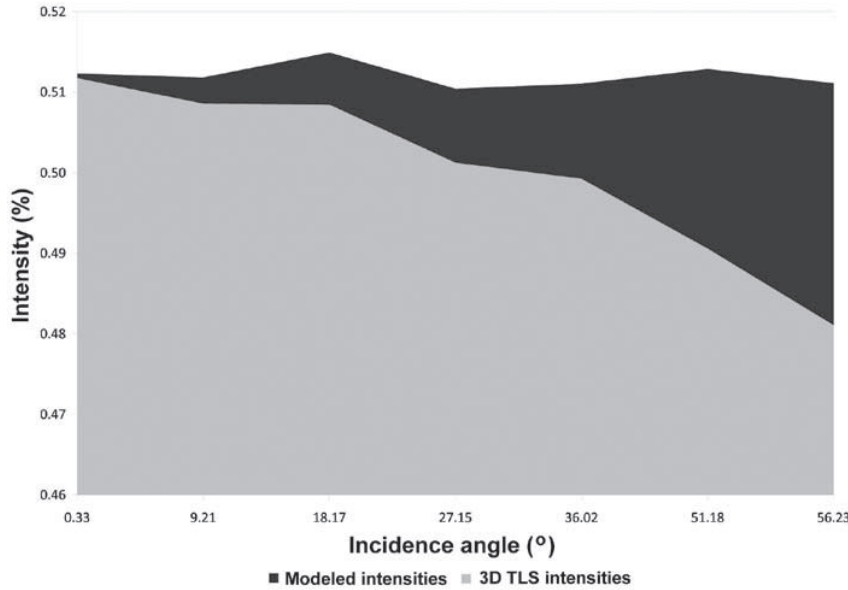


Table 2: Comparison between the results of the measured and uncorrected intensities.

	Standard deviation [%]	Mean intensity [%]
Measured values	1.1	50.01
Modelled values	0.15	51.20

0.3° and 57.5°. Similar to the modelling approach in the previous section, a reference intensity value was used, which showed the smallest angular deviation compared to a normal projection. The differences between this reference value and all other measured intensities were calculated. Finally these figures were approximated with a polynomial approach (Jaeger et al 2005). Given that the resulting function uses an angle as input parameter a solution had to be found to determine the incident angle for each point. To estimate the incident angle (α) for each laser beam, the point cloud surface was locally approximated with a 3 by 3 filter mask in order to determine the surface normal (Drixler 1993). In a similar manner to Section 2.2, using the least-squares method, the correction term for the effect by the incidence angle (named $CORRECTION_{surface}$) is formulated:

$$CORRECTION_{surface} \sim 1.147 \times 10^{-8} \times \alpha^4 - 1.254 \times 10^{-6} \times \alpha^3 + 4.497 \times 10^{-5} \times \alpha^2 - 2.345 \times 10^{-4} \times \alpha + 4.695 \times 10^{-4} \quad (3)$$

where α is the incidence angle of the laser beam to the surface of the object. Figure 2

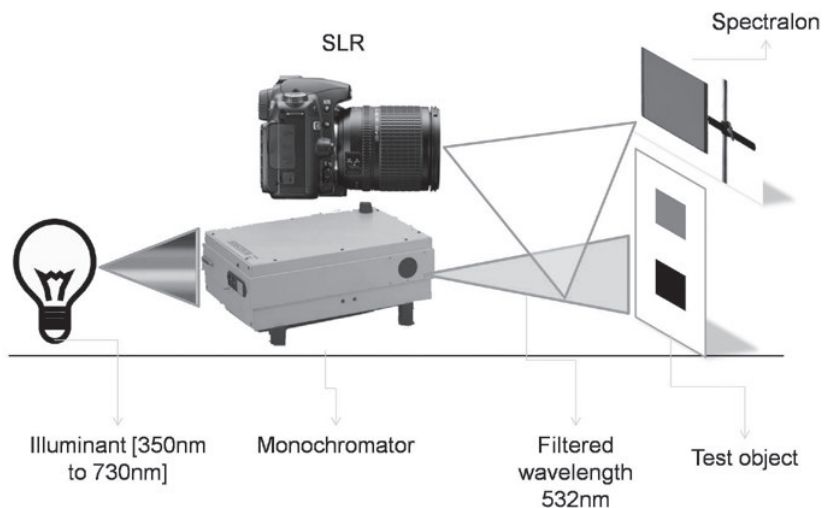
shows the effect of this influence compared to corrected intensity values. The incidence angle α has to be inserted into this equation in the unit of ‘gon’. Note that ‘gon’ can be converted to angles by multiplying by -0.9048 . The statistical results of the two datasets to assess the quality of the modulation are presented in Table 2, where the reference intensity was 51.17%.

Experiment III (Radiometric property v. intensity) and the proposed intensity model

When observing intensity values of practical datasets it is quite obvious that the behaviour of these values is not linear. The aims of this experiment were to discover the radiometric characteristics of the scanner, and to describe a model that transforms intensity values into pseudo quotients of reflexion. To determine the quotients of reflexion on a test object, a camera and a monochromator has been used. This optical instrument uses optical grids to filter certain wavelengths out of a given light source. As the 3D laser scanner used a wavelength of 532nm, the projection of the scanner onto the test object was simulated by the monochromator. A planar wooden board has been used as a test object. To capture a wide radiometric range of output from the instrument, squares were painted on the board that gradually ranged from black to white in different tones of grey. A spectralon panel with a known quotient of reflexion for the used wavelength was used as a reference value. Spectralon is a thermoplastic resin that reacts highly lambertian and reflects more than 99% of incoming radiance (Labsphere 2009).

The spectralon panel, as well as every square on the test object, was irradiated with the monochromator. During each projection of the light beam the irradiated surface was captured with a digital single lens reflex

Figure 3: Schematic description of the experimental setup.



camera. The shutter speed was fixed during the experiment to receive consistent results. Measurement of the grey scale values of the light spot on each square were compared with the value for the spectralon, in order to derive comparative values for the squares. Figure 3 shows the set up of the experiment.

The surface of the test object was then scanned with the 3D laser scanner. Recorded intensity values of the scanner, however, only ranged from roughly 40% to 65%. According to the manufacturer, these values are because of the decoder used. By using the two datasets (quotients of reflexion and measured intensities), a calibration function was modelled that transforms intensity values into pseudo coefficients of reflexion. Figure 4 compares the results from the monochromator and the laser scanner for seven measurements.

The estimated polynomial equation (Jaeger et al 2005) is able to handle uncorrected or corrected intensities (i) in percent for values between 43.75% and 51.6% and follows:

$$f(i) \sim -82711.8531xi^4 + 158892xi^3 - 114213.1379xi^2 + 36418.0765xi - 4247.0431 \quad (4)$$

SOFTWARE FOR INTENSITY CORRECTION AND CALIBRATION

In order to apply the cognitions that were mentioned in the previous sections, a

Figure 5: Dataflow in the developed programme.

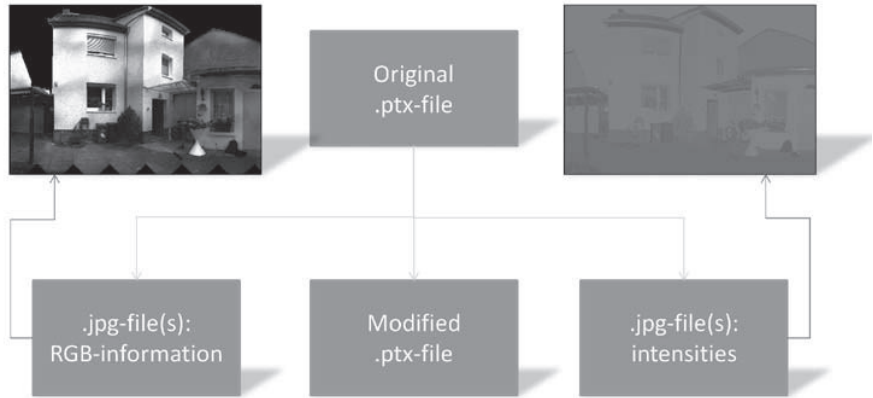


Figure 6: Calibration of the given dataset.

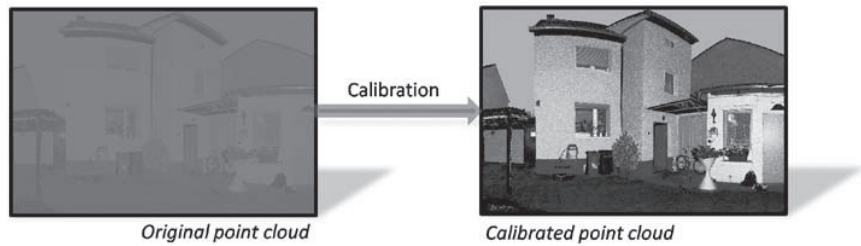


Figure 7: Correction of a calibrated pointcloud.

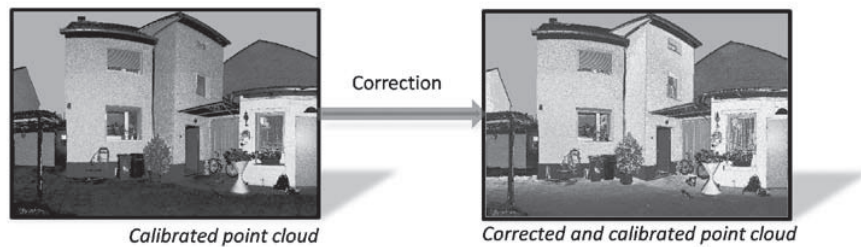
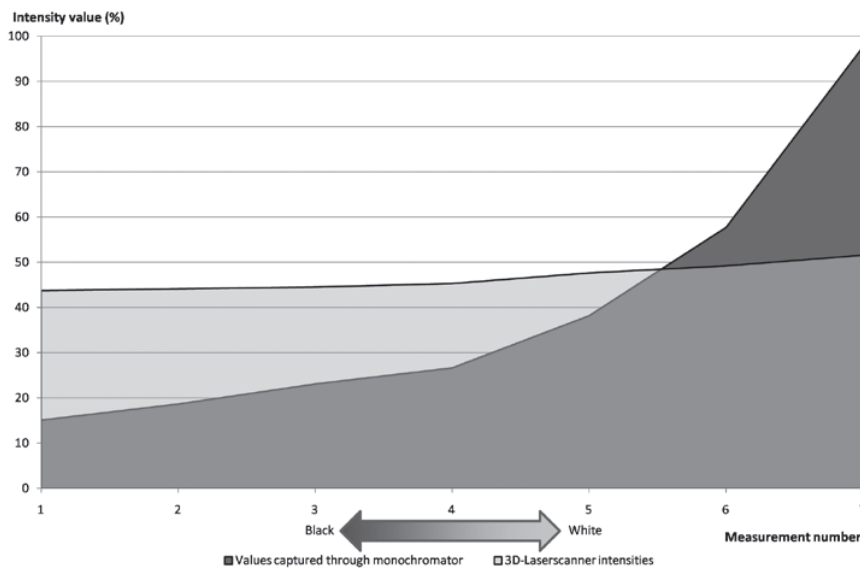


Figure 4: Measured quotient of reflexion and intensities for seven measurements.



software was developed to calibrate and correct a given point cloud. The programme delivers a modified point cloud and at least one image matrix by interpreting the projection matrix of the scanner as an image by using the intensity values as schematically presented in Figure 5.

If the scanner possesses a camera, a second image can be written with the greyscale values. The basis of this function, as well as for approximating the point cloud surface, is *Leica's* ptx-format. It consists of blocks with geometry, intensity and colour information listed in the order the point cloud was measured. If a distance measurement wasn't successful, the structure of the matrix can nevertheless be found by using default values.

For every scan that captures information, a new block is added to the file. The header of each block contains the dimensions of the scanned matrix.

CALIBRATION AND CORRECTION OF A POINT CLOUD

To test the software, a dataset was obtained by scanning a house. The distance between the scanner and the house was about 5m. This distance allowed awkward angles of impact for the upper areas of the building to be included. The scene was scanned with a resolution of about 2cm by 2cm on the house surface, which resulted roughly 210000 points. Figure 6 shows the results of the process that transforms the measured intensities into values of the pseudo quotient of reflexion.

The calibration process causes a visual effect that is similar to stretching, i.e. the contrast increases. As the horizontal distance between the scanner and the object was only about 5m, no damping effects on the intensity due to distance were expected. For this example, only the effect of the incident angle was corrected. Figure 7 shows the result of the calibration and correction process.

The effect of the correction can clearly be seen in the right image of Figure 7. The most important change is the correction of the small side part of the cladding in the middle of the house. After processing, the front looks quite homogeneous. Also important is the correction of the gable in the left part of the image, which had characteristics that were similar to the cladding of the building.

Figure 8: Segmentation of the calibrated point cloud [left] and the calibrated and corrected dataset [right].



SEGMENTATION OF POINT CLOUDS

The pictures shown in Figure 8 were processed with a segmentation algorithm, which uses the statistical ISODATA method (Ball et al 1965). This algorithm is mostly used in image processing to divide the content into different groups. The cladding was divided into three classes: one for bright claddings (light grey); one for the dark gable in the right image part (dark grey); and one for values in between (grey).

After correction, the front of the house falls mostly within the light grey class. The gable in the left part of the picture was classed as grey before correction, and as light grey after correction (as expected). The dark gable in the right image appears “noisy” after correction, which can be attributed to its rough surface. The transition between the grey and the dark grey classes on the courtyard after correction are a result of incident angles that are beyond the valid values.

VERIFICATION OF ACCURACY

After considering all influences on the final intensity values separately, a clearer idea of the accuracy achieved can be obtained by presenting the errors in a summarised version. Two summarising variances are calculated: one without any compensation of the mentioned influences, and one that used all modelled correction values. Gaussian errors are used to determine this variable:

$$dY = \frac{\partial \varphi}{\partial X_1} \cdot dX_1 + \frac{\partial \varphi}{\partial X_2} \cdot dX_2 + \dots + \frac{\partial \varphi}{\partial X_m} \cdot dX_m \tag{5}$$

The parameter dY describes the standard deviation that results from the functional connectivity between the particular parameters X_m .

Distance effects have a standard deviation of 2.6% (for an analysed object distance between 10m and 200m). This was reduced to 0.5% by using the correction values from the estimated polynomial function Equation (2). The deviation from the normal incidence angle has a standard deviation of 1.1% (for angles between 0° and 56.7°). After using the

Table 3: Summary of the standard deviations.

	Standard deviation of intensity [%]	Measured standard deviation [%]	Standard deviation after correction [%]	Resulting, measured standard deviation [%]	Resulting, corrected standard deviation [%]
Influence through the measured distance	0.2	2.6	0.5	2.61	0.53
Influence through the incidence angle	0.2	1.1	0.15	1.12	0.25
Influence of measured distance and incidence angle	0.2	2.6 + 1.1	0.5 + 0.15	2.83	0.56

correction value Equation (3), the standard deviation was narrowed to 0.15%. Because they are statistical errors, instead of Equation (5), the standard deviations are combined using the expression:

$$\Delta z = \sqrt{(\Delta x)^2 + (\Delta y)^2} \quad (6)$$

Eq. (6) can be used for additive functions with arbitrary many terms; Δz describes the resulting standard deviation that was calculated by using the given standard deviations, here represented by Δx and Δy . Because no details about the standard deviation of the intensity value are published, it was estimated as 0.2%.

From Table 3, it appears that the effect of distance is larger than that of the incidence angle. In practice this circumstance is reversed because arbitrary surfaces can be found in the real world. Edges and holes can cause large correction values that falsify the intensity and raise the standard deviation of a homogenous surface.

SUMMARY

It has been shown that the intensity value supplies an alternative information source that could be used for segmentation or general visualisation purposes. Modelling with the aid of polynomial functions showed no noteworthy variations. With the help of implemented software, a tool is now available that can compensate for the effects of distance between the scanner and target, as well as the variation of the incidence angle. The intensities can also be transformed into pseudo quotients of reflexion by using the proposed calibration function. All introduced functions are only suitable for the analysed instrument.

The method was primarily developed to offer distinguishable features that can be used for segmentation or classification purposes. Practical application fields can, for example, be found in mining, architecture, robotics or in preservation of historical monuments. Follow up research will try to use corrected intensity values for tracking of objects when using a 3D time of flight camera. Also the combined use of geometric and radiometric

information in knowledge bases for detection purposes will be analysed.

An influencing factor on intensity not mentioned is humidity. Research into multispectral scanning systems (Hemmler 2006) suggest that future developments could combine this technique with conventional 3D-Laserscanners to capture more information about the irradiated material. This data could then be used to compensate the influence through humidity.

ACKNOWLEDGEMENTS

The author would like to express his gratitude to Dr. Kwang-Ho Bae, Dr. David Belton and Kwanthar Lim in the Department of Spatial Sciences at Curtin University of Technology, Australia, for their comments and assistance on this manuscript.

i3mainz, University of Applied Sciences Mainz, Germany: Furthermore I have to thank my former colleagues M.Eng. Uwe Huxhagen and M.Eng. Andreas Marbs for heaps of help over the past years. M.Sc. Rainer Schütze and M.Sc. Burkhard Tietz showed me lots of helpful material when I was programming on this project. Also I have to thank Prof. Dr.-Ing. Frank Boochs, M.Eng. Guido Heinz, Prof. Dr.-Ing. Fredie Kern and Prof. Dr.-Ing. Jörg Klonowski for sharing their knowledge with me.

Dr. Sebastian Schmidt (University of Colorado, USA) and Prof. Dr. Manfred Wendisch (University of Leipzig, Germany) helped me out with instruments that I've used for radiometric experiments and gave me much theoretic input. Thanks a lot for that.

I'd like to thank Markus Mettenleiter at Zoller + Fröhlich, Germany for giving me helpful hardware hints. Katja Bartolomae, Marion Grosse-Elshoff and Ulf Karnagel at Leica Europe gave me details about some of the Leica formats that I have used while programming.

Special thanks go to Michaela Plein for her patience with me over the years.

REFERENCES

- Bae, K.-H., Belton D. and Lichti, D. D. 2007. Pre-processing procedures for raw point clouds from terrestrial laser scanners. *Journal of Spatial Science*, 52(2): 65-74.
- Ball, G. and Hall, D. 1965. ISODATA, A novel method of data analysis and pattern classification. Technical Report AD 699616, Stanford Research Institute, Menlo Park, CA, 1965.
- Belton, D. 2008. Classification and Segmentation of 3D point clouds, PhD thesis, Department of Spatial Sciences, Curtin University of Technology, 164p.
- Boehler, W. and Marbs, A. 2004. 3D scanning and photogrammetry for heritage recording: a comparison. *Geoinformatics 2004 Proc. 12th Int. Conf. on Geoinformatics*. University of Gävle, Sweden.
- Drixler, E. 1993. Analyse der Form und Lage von Objekten im Raum. Munich, Germany: Deutsche Geodätische Kommission, Heft Nr. 409.
- Gordon, S. J. 2005. Structural deformation measurement using terrestrial laser scanners, PhD thesis, Department of Spatial Sciences, Curtin University of Technology, 229p.
- Hancock, J., Hebert, M. and Thorpe, C. 1998. Laser Intensity-Based Obstacle Detection. International Conference on Intelligent Robot and Systems. Victoria, B.C., Canada.
- Hemmler, M., Weritz, F. and Maierhofer, C. 2006. Multispektraler Laserscanner – Einsatz eines multispektralen Laserscanners zur Untersuchung von Bauwerksflächen. IRB Verlag, Stuttgart.
- Hoefle, B., Geist, T., Rutzinger, M. and Pfeifer, N. 2007. Glacier Surface Segmentation Using Airborne Laser Scanning Point Cloud and Intensity Data. *IAPRS*, Vol. XXXVI, Part 3/W52.
- Hoefle, B. and Pfeifer, N. 2007. Correction of Laser Scanning Data: Data and model-driven Approaches. *IAPRS*, Vol. XXXVI, Part 3/W52.
- Jäger, R., Müller, T., Saler, H. and Schwäble, R. 2005. Klassische und robuste Ausgleichungsverfahren. Wichmann Verlag, Heidelberg.
- Kaasalainen, S., Hyypää, J., Litkey, P., Hyypää, H., Ahokas, E., Kukko, A. and Kaartinen, H. 2007. Radiometric Calibration of ALS Intensity. *IAPRS*, Vol. XXXVI, Part 3/W52.
- Kern, F. 2003. Automatisierte Modellierung von Bauwerksgeometrien aus 3D-Laserscanner-Daten. Braunschweig: Geodätische Schriftenreihe der Technische Universität Braunschweig, Heft 19, (Dissertation), 164p.
- Labsphere 2009. Labsphere::Materials and Coatings::Spectralon. In: <http://www.labsphere.com/productdetail.aspx?id=226>. Accessed: 27.07.09.
- Lichti, D. and Harvey, B.R. 2002. The Effects of Reflecting Surface Material Properties on Time-of-

Flight Laser Scanner Measurements. Symposium on Geospatial Theory, Processing and Applications. Ottawa, Canada.

Lichti, D. 2005. Spectral filtering and classification of terrestrial laser scanner point clouds. *The Photogrammetric Record*, 20 (111): 218–240 (23)

Pfeifer, N., Dorninger, P., Haring, A. and Fan, H. 2007. Investigating Terrestrial Laser Scanning Intensity Data: Quality and Functional Relations. *In*: Gruen, A. and Kahmen, H. (eds.) International Conference on Optical 3D-Measurement Techniques VIII, Zürich, Switzerland.

Wang, C. and Lu, Y. 2009. Potential of ILRIS3D Intensity Data for Planar Surfaces Segmentation. *Sensors*, 9: 5770-5782.